



Hydrogeochemical Processes and Inverse Modeling for a Multilayer Aquifer System in the Yuaner Coal Mine, Huaibei Coalfield, China

Miao Zhang^{1,2} · Luwang Chen² · Duoxi Yao¹ · Xiaowei Hou² · Jie Zhang² · Hao Qin² · Xingxing Ren² · Xin Zheng²

Received: 21 August 2021 / Accepted: 14 February 2022 / Published online: 25 February 2022
© The Author(s) under exclusive licence to International Mine Water Association 2022

Abstract

Coal mining can dramatically change hydrogeological conditions and induce serious environmental problems. Fifty groundwater samples were collected from the main aquifers in the Yuaner coal mine (Anhui Province, China). The results show that the main hydrogeochemical processes in the mine include dissolution, precipitation, pyrite oxidation, desulfurization, and cation exchange. The Neogene porous aquifer is affected by groundwater flow conditions; its main hydrogeochemical processes are dissolution of carbonate minerals and gypsum, and cation exchange. The Permian coal measure's fractured sandstone aquifer was confirmed to be controlled by the region's geological structure; its main hydrogeochemical processes are desulfurization and cation exchange. The Carboniferous Taiyuan limestone aquifer was determined by both groundwater flow conditions and regional geological structure; its main hydrogeochemical processes are dissolution of carbonate minerals and gypsum, pyrite oxidation, and cation exchange. Additionally, hydrogeochemical inverse modeling of the groundwater flow path confirm the hydrochemistry results and principal component analysis.

Keywords Groundwater systems · Major ion chemistry · Conventional hydrochemistry methods · Principal component analysis

Introduction

North China accounts for more than 60% of China's total coal production, but due to multi-stage tectonics, its associated hydrogeological conditions are extremely complex (Han et al. 2013). Groundwater is the main domestic water for local residents because it is more economical and reliable than surface water and is not easily polluted by the external environment (Li et al. 2021; Wang et al. 2020). However, significant interplay exists between coal mining and groundwater resource management (Chen et al. 2017). Long-term mining activities change the flow path of groundwater and enhance hydraulic connections among aquifers (Li et al. 2018). Moreover, mining can adversely affect groundwater quality and cause hydrochemical anomalies. Recently, deep coal mining has induced increasingly prominent water

quality problems (Bridge et al. 2004; Huang et al. 2017). Better understanding of these hydrogeochemical processes and their controlling factors is important for sustainable management and long-term utilization of the area's groundwater resources.

Many methods have been successfully used to study hydrogeochemical processes in multilayer aquifer systems. Conventional hydrochemistry methods, such as Piper diagram, ion ratio analysis, and Gibbs plots, are widely used in the study of groundwater formation mechanisms and hydrochemical types (Chotpantarat et al. 2021; Li et al. 2013; Vaiphei et al. 2021). Multivariate statistical analysis methods, such as principal component analysis and cluster analysis, have also been applied (Wu et al. 2020; Yang et al. 2021). Moreover, isotope tracking techniques, such as δD , $\delta^{18}O$, and $\delta^{34}S$, have proven to be useful tools for tracing the pollution sources within surface water and groundwater (Kaown et al. 2021; Malov et al. 2019; Qian et al. 2013). With the development of computer technology, quantitative analysis methods, such as hydrogeochemical simulation, are becoming more and more popular in groundwater studies because of their power in reverse identification and prediction (Ibrahim 2020; Taufiq et al. 2018; Zhang et al.

✉ Luwang Chen
luwangchen888@163.com

¹ School of Earth and Environment, Anhui University of Science and Technology, Huainan 232001, China

² School of Resources and Environmental Engineering, Hefei University of Technology, Hefei 230009, China

2021). Previous studies have found that the chemical components can provide groundwater evolutionary information and determine the hydrogeochemical processes (Paternoster et al. 2021; Sako et al. 2016). Furthermore, concentration variations of major ions is easier to determine than trace ions, which are commonly used to evaluate hydrogeochemical processes (Belkhiri et al. 2013; Zhang et al. 2020). For example, Li et al. (2018) revealed the hydraulic connectivity of multilayer aquifers by hydrochemistry and a hydraulic connectivity index. Wu et al. (2015) investigated the impacts of groundwater pumping-induced hydraulic leakage on groundwater geochemistry and showed that leakage from adjacent aquifers can be very important in altering groundwater quality in a target aquifer. Zhang et al. (2019a) studied the hydrogeochemical processes of a mining area with a karst collapse column using major ions and stable isotopes, which revealed that the collapse column was a potential water channel. Ismail et al. (2021) used major ions to analyze the hydrochemical characteristics of groundwater and used maps showing the spatial variations of different groundwater quality parameters to analyze its spatial evolution. Qiao et al. (2019) used principal component analysis along with hydrogeochemical methods to determine the hydrochemical evolution of groundwater during coal mining, and found significant differences in hydrogeochemical processes among aquifers. This is because the hydrogeochemical processes are

mainly controlled by natural processes, such as hydrogeological conditions, aquifer lithology, and water–rock interaction (Banning et al. 2013; Hu et al. 2018). These studies mainly focused on identifying the hydrogeochemical processes or simply evaluating chemical properties of groundwater, rarely considering the spatial distribution and factors controlling the hydrogeochemical processes in coal mining areas.

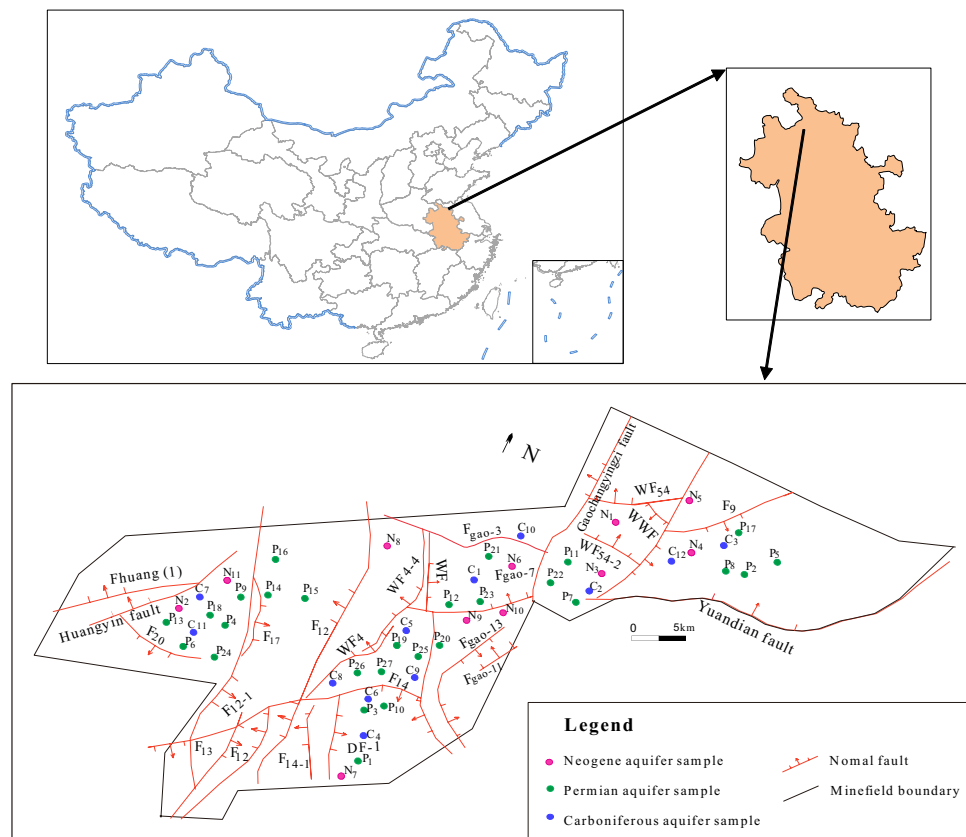
In this study, we examined the hydrogeochemical processes of the porous Neogene aquifer, the fractured Permian sandstone aquifer, and the Carboniferous limestone aquifer in the Yuaner coal mine using principal component analysis, Piper diagrams, Gibbs plot, ion ratio analysis, and hydrogeochemical inverse modeling. We analyzed the aquifers' hydrogeochemical characteristics and major ions sources, and explored the spatial distribution and factors controlling the groundwater's hydrogeochemical processes.

Materials and Methods

Geological Setting

The study area, the Yuaner coal mine, is located southwest of the Huaibei coalfield, in Anhui Province, China (Fig. 1). The terrain is relatively flat and slightly inclined to the southeast. The study area is 10.9–13.3 km long from east to

Fig. 1 Map of geological and sampling distribution of the study area



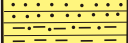
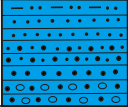
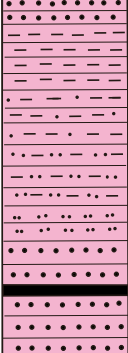
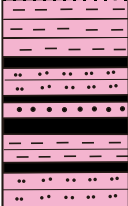

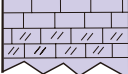
west and 1.3–5.3 km wide from north to south, with a total area of $\approx 41.9 \text{ km}^2$. During the period of 1998–2020, the annual average temperature was 13.8°C and the annual average precipitation was 834 mm. The precipitation is mainly concentrated in June, July, and August, accounting for about 50% of the total annual precipitation.

Due to the effects of the Yuandian, Gaochangyingzi, and the Huangyin faults, the overall strike of the study area is near east–west and north inclined monoclinic fault block, with a small dip angle of $5^\circ \sim 15^\circ$ (Zhai et al. 2013; Zhu et al. 2018). Small geological structures exist in the mining area. The full sedimentary sequence is shown in Fig. 2; from old to new, the Neogene, Permian, Carboniferous, and Ordovician strata. The main coal-bearing strata are the Upper and Lower Permian and Carboniferous formations. The Upper Permian strata is 598–709 m thick, averaging 680 m. It is comprised of sandstone, mudstone, siltstone, and coal seams. The Lower Permian strata is 282–433 m thick, averaging 330 m. It is comprised of sandstone, mudstone, and coal seams. The total thickness of Permian coal-bearing strata is about 900 m, with a coal-bearing coefficient of 1.6%. The minable coal seams in this part are 3_2 , 7_2 , 8_1 ,

8_2 , and 10, from top to bottom, and the main mining coal seams are 7_2 and 10. The thickness of the Carboniferous strata is 110–150 m, averaging 120 m. It is comprised of limestone, sandstone, and thin coal seams. Based on the lithology, aquifer media, and burial depth, the four main water-inrush aquifers are:

- (1) The confined Neogene loose porosity aquifer (referred to as the Neogene aquifer) is composed of sand, gravel, and at the bottom, a clay layer. The sediments mainly consist of silicate and carbonate minerals, and gypsum.
- (2) The Permian coal-measure fissured sandstone aquifer (referred to as the Permian aquifer) is composed of sandstone, mudstone, coal seams, and siltstone; as a whole, its water yield property is weak. Generally, there is no hydraulic connection between the sandstone layers and coal seams. The Permian aquifer is a confined aquifer with favorable storage capacity, which may have hydraulic connections due to water-conducting structures and mining fractures. This aquifer is recharged by both inter-layer runoff and slow infiltration of the Neogene aquifer in the shallow outcrop zone.

Fig. 2 Stratigraphic column of the study area

Epoch	Thickness(m) Range Average	Stratum	Lithology
Quaternary	$\frac{78.6 \sim 106.2}{87.2}$		Sand, clay
Neogene	$\frac{15.45 \sim 203.2}{124}$		Sand, clay, gravel
Upper Permian	$\frac{598 \sim 709}{680}$		Sandstone, mudstone, siltstone and coal seams 3_2 is the main minable coal seam
Lower Permian	$\frac{282 \sim 433}{330}$		Sandstone, mudstone and coal seams 7_2 , 8_1 , 8_2 and 10 are the minable coal seams
Carboniferous	$\frac{110 \sim 150}{120}$		Limestone, sandstone and coal seams
Ordovician	>500		Limestone, dolomite limestone

- (3) The Carboniferous Taiyuan limestone aquifer (referred to as the Carboniferous aquifer) includes limestone, mudstone, sandstone, siltstone, and a thin coal seam, and contains unevenly distributed pyrite nodules. The development of karst fissures and the water yield are both heterogeneous. The Carboniferous aquifer is recharged by the Neogene aquifer in the shallow outcrop zone.
- (4) The Ordovician limestone aquifer (referred to as the Ordovician aquifer) is composed of brown, grayish-brown, and light pink thick-bedded limestone with a minor amount of pyrite nodules at the top. The shallow karst is a confined aquifer with developed karst fissures and rich water content. The Ordovician aquifer is far away from the coal-bearing strata, with limited hydrochemical data and few hydrogeological boreholes. Therefore, this study mainly focused on the three other aquifers.

Samples and Methods

Fifty groundwater samples were collected from the Yuaner mine from 2012 to 2020, including 11 samples from the Neogene aquifer, 27 samples from the Permian aquifer, and 12 samples from the Carboniferous aquifer. These samples were taken from drainage holes, hydrological observation holes, working faces, and underground tunnels; detailed locations are displayed in Fig. 1. The measured indices include the concentrations of Na^+ and K^+ (due to the low K^+ content in the study area, the K^+ was combined with the Na^+), Ca^{2+} , Mg^{2+} , Cl^- , SO_4^{2-} , HCO_3^- , TDS (total dissolved solids), and pH.

The 50 samples were collected in polyethylene bottles, using standard cleaning and filtration procedures before sampling, and then sealed for testing. The Na^+ , K^+ , Ca^{2+} ,

and Mg^{2+} were measured by inductively coupled plasma emission spectrometry (Thermo Fisher Scientific), with a detection limit of 0.02 mg/L. Cl^- and SO_4^{2-} were measured by ion chromatography (ICS-600–900), HCO_3^- by titration; the detection limit for all was 5 mg/L. The pH was measured by the glass electrode method (ST20T-B handheld portable instruments). TDS was obtained by summing the contents of various conventional components and subtracting 1/2 of the HCO_3^- concentration (Guo et al 2020). The accuracy of the results was tested by the following formula (Shen et al. 1999),

$$E = \frac{\sum m_c - \sum m_a}{\sum m_c + \sum m_a} \times 100\% \quad (1)$$

where: E is the relative error, m_c and m_a are the Mg equivalent concentrations of cations and anions, which are expressed in meq/L, respectively. The ionic balance errors of all groundwater samples collected were within $\pm 5\%$, as shown in supplemental Table S-1.

Results

Hydrochemical Characteristics

The hydrochemical indices of the groundwater samples are presented in Table 1. The average pH of each aquifer was > 8 , which means that the groundwater was all alkaline or weakly alkaline. The average concentrations of the major ions in the Neogene aquifer was $\text{Na}^+ > \text{Ca}^{2+} > \text{Mg}^{2+}$, $\text{HCO}_3^- > \text{SO}_4^{2-} > \text{Cl}^-$. The order of cations and anions in the Permian and Carboniferous aquifers was $\text{Na}^+ > \text{Ca}^{2+} > \text{Mg}^{2+}$, $\text{HCO}_3^- > \text{Cl}^- > \text{SO}_4^{2-}$, indicating that the two aquifers have similar hydrochemical processes.

Table 1 Summary statistics of hydrogeochemical variables

Aquifer	Index	pH	Na^+ (mg/L)	Ca^{2+}	Mg^{2+}	Cl^-	SO_4^{2-}	HCO_3^-	TDS
Neogene aquifer (n = 11)	Max	8.67	392.52	53.85	46.58	306.16	314.46	620.4	1248.27
	Min	7.76	303.53	26.23	21.13	198.54	165.46	446.82	1028.6
	Mean	8.07	347.54	38.42	33.22	244.84	253.83	487.07	1161.40
	C_v (%)	3.39%	7.57%	21.02%	19.30%	16.91%	18.73%	10.72%	4.66%
Permian aquifer (n = 27)	Max	8.9	413.01	47.5	29.28	326.31	276.6	638.07	1017.805
	Min	7.46	212.98	3.22	1.95	95.25	2.06	131.8	547.93
	Mean	8.25	313.49	13.06	10.30	207.72	70.33	429.17	829.48
	C_v (%)	5.56%	18.17%	81.87%	72.48%	27.57%	86.53%	23.16%	14.83%
Carboniferous Aquifer (n = 12)	Max	8.5	353.1	94.85	53.45	282.21	224.32	538.2	995.3
	Min	7.37	127.49	11.11	13.48	44.04	26.34	314.5	556.56
	Mean	7.99	223.09	48.49	32.28	192.64	121.35	394.02	814.87
	C_v (%)	4.46%	31.15%	57.83%	44.09%	37.89%	58.25%	17.89%	14.78%

The SO_4^{2-} concentration in the Permian aquifer was less than in the Neogene and Carboniferous aquifers, while the HCO_3^- concentration was greater than in the Neogene and Carboniferous aquifers. This may be due to desulfurization, which reduces SO_4^{2-} concentrations, but increases HCO_3^- concentrations (Huang et al. 2017b).

The coefficient of variation (C_v) is an index of data dispersion (Zhang et al. 2019a). The greater the C_v , the stronger the variability. The C_v of the Neogene and Carboniferous aquifers were less than 60%, which indicates that the variability of the Neogene and Carboniferous aquifers is moderate and the hydrogeochemical process is relatively stable. The C_v of Ca^{2+} , Mg^{2+} , and SO_4^{2-} in the Permian aquifer are 81.87%, 72.48%, and 86.53%, respectively, which indicates that this aquifer is disturbed and its hydrogeochemical process is complex.

Piper trilinear diagrams are frequently used to determine hydrochemical types of groundwater (Fijani et al. 2017; He et al. 2020). In the Neogene aquifer, the main cation was Na^+ and the main anions were HCO_3^- and Cl^- ; the main hydrochemical types were $\text{HCO}_3\text{-Na}$, $\text{HCO}_3\text{-Cl-Na}$, $\text{Cl-HCO}_3\text{-Na}$, and Cl-Na (Fig. 3). The Na^+ in groundwater increased gradually from the Neogene to the Permian aquifer; in the Permian aquifer, Na^+ was the main cation, HCO_3^- and Cl^- were the main anions, and the main hydrochemical types were $\text{HCO}_3\text{-Na}$, $\text{HCO}_3\text{-Cl-Na}$, and $\text{Cl-HCO}_3\text{-Na}$. In the Carboniferous aquifer, Na^+ and Ca^{2+} were the main cations, HCO_3^- and Cl^- the main

anions; the main hydrochemical types were $\text{Cl-HCO}_3\text{-Na}$, $\text{HCO}_3\text{-Na}$, Cl-Na , $\text{HCO}_3\text{-Na-Ca}$, and $\text{HCO}_3\text{-Cl-Na}$.

Hydrogeochemical Process Determination

Gibbs Plot

Gibbs plots were initially used to determine the evolution surface water chemistry, but has also been used to analyze the formation mechanism (Huang et al. 2017; Marandi et al. 2018; Tian et al. 2020). In the Gibbs plots, if the TDS value is high and $\text{Na}^+ / (\text{Na}^+ + \text{Ca}^{2+})$ or $\text{Cl}^- / (\text{Cl}^- + \text{HCO}_3^-)$ is also high (close to 1), the ion-controlling mechanism is evaporative crystallization. If the TDS value is medium and $\text{Na}^+ / (\text{Na}^+ + \text{Ca}^{2+})$ or $\text{Cl}^- / (\text{Cl}^- + \text{HCO}_3^-)$ is less than 0.5, the ion controlling mechanism is water–rock interaction. If the TDS value is low and $\text{Na}^+ / (\text{Na}^+ + \text{Ca}^{2+})$ or $\text{Cl}^- / (\text{Cl}^- + \text{HCO}_3^-)$ is close to 1, the hydrochemistry is dominantly that of precipitation.

As shown in Fig. 4a, the $\text{Na}^+ / (\text{Na}^+ + \text{Ca}^{2+})$ in groundwater samples ranged from 0.6 to 1.0, and the content of Na^+ was much greater than that of Ca^{2+} . According to Fig. 4b, the $\text{Cl}^- / (\text{Cl}^- + \text{HCO}_3^-)$ ranged from 0.1 to 0.6, and the groundwater samples were distributed in the water–rock interaction region, indicating that the hydrochemistry in the study area is mainly controlled by water–rock interactions.

Fig. 3 Piper diagram of the groundwater samples from different aquifers

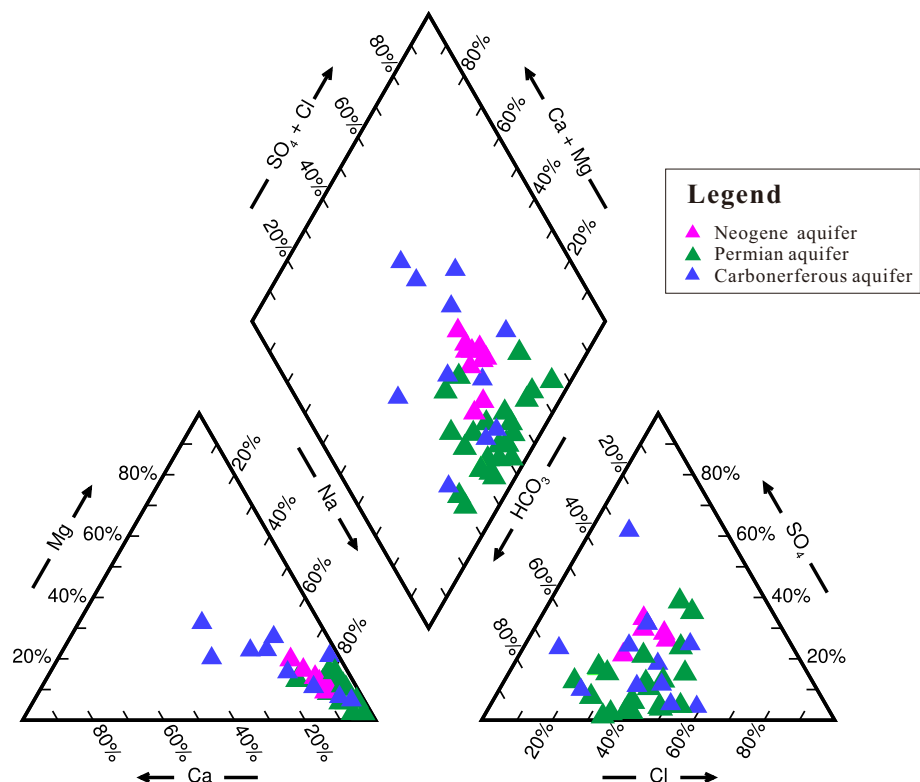
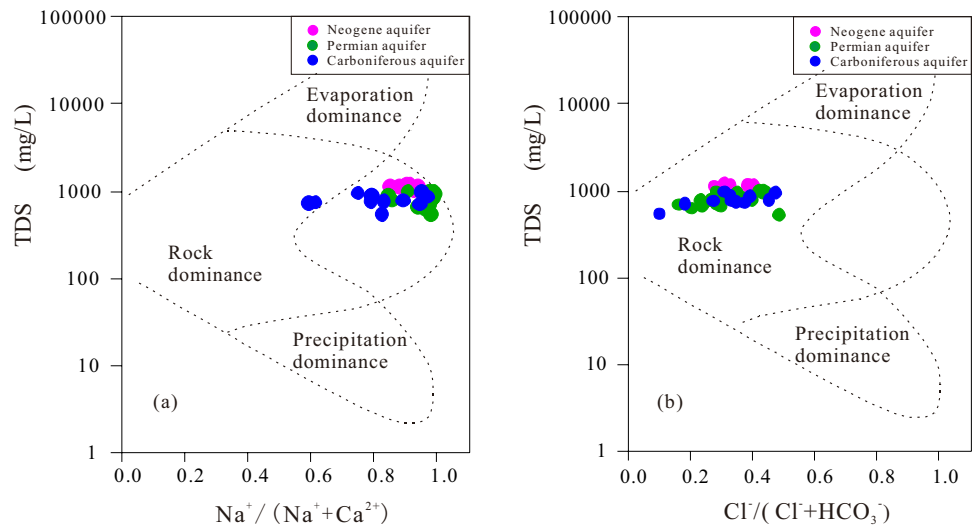


Fig. 4 Gibbs plots of the groundwater samples in the study area

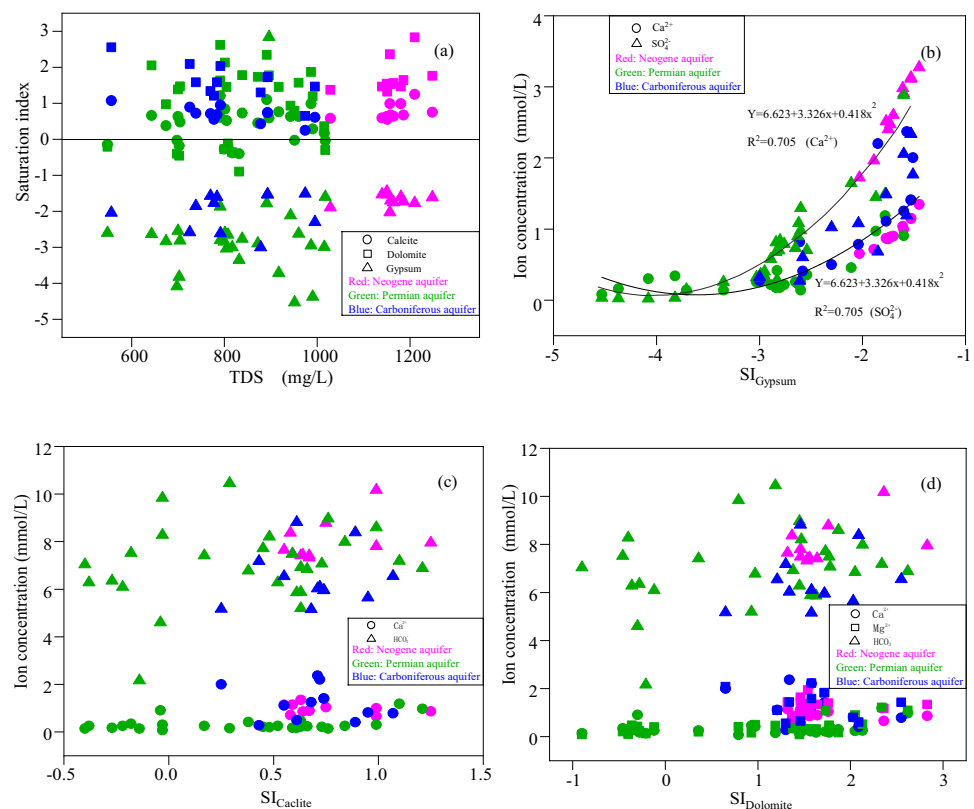


Saturation Index (SI)

SI values indicate whether minerals are soluble in water (Luan et al. 2019). The SI values of the potential reactive minerals in the study area aquifers were calculated by PHREEQC 3.0 (Table S-1). The ranges of SI for calcite and dolomite were 0.55–1.25 and 1.32–2.83 in the Neogene aquifer, -0.4 – 1.21 and -0.46 – 2.64 in the Permian aquifer, and 0.25 – 1.07 and 0.65 – 2.55 in the Carboniferous

aquifer. The SI for gypsum in all groundwater samples was less than 0. In a closed homogeneous aquifer, TDS usually increases due to the gradual dissolution of minerals (Chen et al. 2017). However, the SI_{Calcite} , SI_{Dolomite} , and SI_{Gypsum} in the three aquifers did not correlate with TDS (Fig. 5a). Gypsum dissolution exponentially increases the concentration of Ca^{2+} and SO_4^{2-} ; the correlation coefficients between Ca^{2+} and SI_{Gypsum} , SO_4^{2-} , and SI_{Gypsum} were 0.72 and 0.67, respectively (Fig. 5b). In addition, the Ca^{2+} , Mg^{2+} ,

Fig. 5 **a** Correlations of TDS and SI_{Gypsum} , SI_{Calcite} , SI_{Dolomite} , **b** correlations of SI_{Gypsum} and Ca^{2+} , SO_4^{2-} , **c** correlations of SI_{Calcite} and Ca^{2+} , HCO_3^- , **d** correlations of SI_{Dolomite} and Ca^{2+} , Mg^{2+} , HCO_3^-

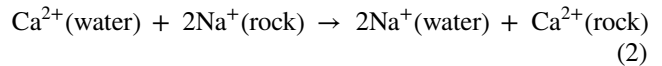


and HCO_3^- concentrations do not correlate with $\text{SI}_{\text{Calcite}}$ or $\text{SI}_{\text{Dolomite}}$ (Fig. 5c, d), which means that calcite and dolomite would not continue to dissolve in the groundwater.

Ions Ratio Analysis

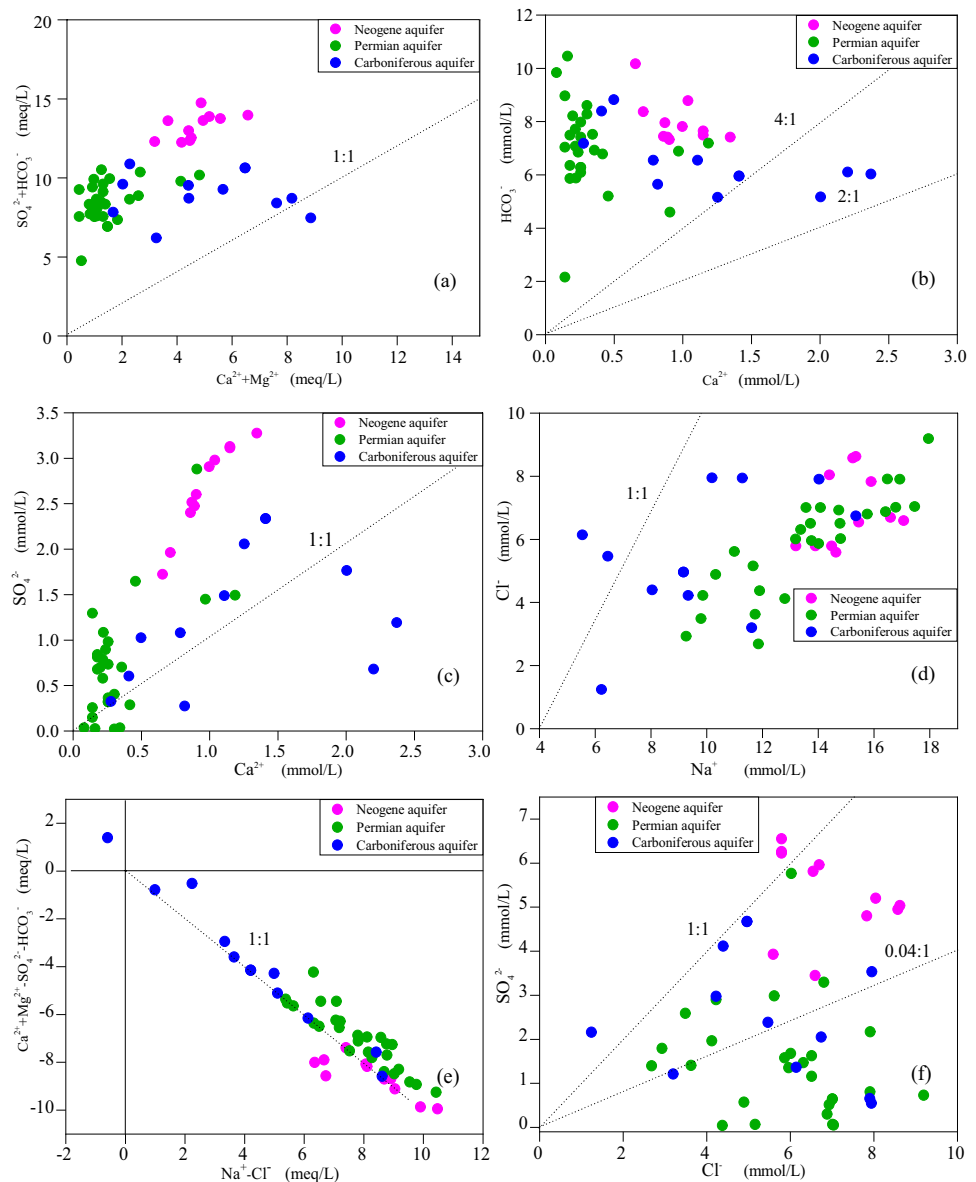
Ions ratio analysis is frequently used to explore the source of major ions and possible hydrogeochemical processes. When Ca^{2+} and Mg^{2+} in groundwater mainly come from dissolution of carbonate minerals and gypsum, $\rho(\text{Ca}^{2+} + \text{Mg}^{2+})/\rho(\text{SO}_4^{2-} + \text{HCO}_3^-) = 1$ (Gastmans et al. 2010; Kumar et al. 2020). As shown in Fig. 6a, except for one groundwater sample from the Carboniferous aquifer, the groundwater samples are above the 1:1 line, meaning that Ca^{2+} and Mg^{2+} are insufficient. In addition to Ca^{2+} and Mg^{2+}

produced by dissolution of carbonate minerals and gypsum, cation exchange can release Na^+ from the rock and remove Ca^{2+} and Mg^{2+} (Eq. 2).

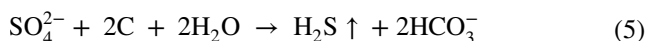
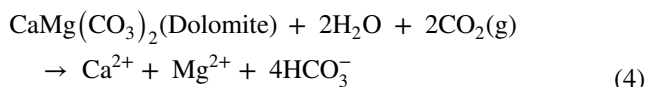


Many studies have shown that Ca^{2+} and HCO_3^- in groundwater mainly come from carbonate mineral dissolution (Zhang et al. 2019b, c). If Ca^{2+} and HCO_3^- in groundwater are only produced by calcite dissolution, then $\rho(\text{HCO}_3^-)/\rho(\text{Ca}^{2+})$ should be 2:1 (Eq. 3). If Ca^{2+} and HCO_3^- are only produced by dolomite dissolution, then $\rho(\text{HCO}_3^-)/\rho(\text{Ca}^{2+})$ should be 4:1 (Eq. 4). As shown in Fig. 6b, there are three main areas below the 2:1 line and no

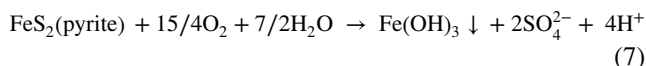
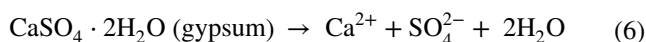
Fig. 6 Scatter plots of major ions: **a** $\text{Ca}^{2+} + \text{Mg}^{2+}$ and $\text{SO}_4^{2-} + \text{HCO}_3^-$ concentration; **b** Ca^{2+} and HCO_3^- concentration; **c** Ca^{2+} and SO_4^{2-} concentration; **d** Na^+ and Cl^- concentration; **e** $\text{Na}^+ - \text{Cl}^-$ and $\text{Ca}^{2+} + \text{Mg}^{2+} - \text{SO}_4^{2-} - \text{HCO}_3^-$ concentration; **f** Cl^- and SO_4^{2-} concentration



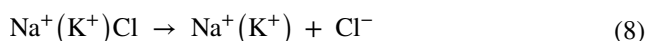
groundwater sample in the region where HCO_3^- is deficient. The range of 1–4:1 is a transition region and three groundwater samples from the Carboniferous aquifer are distributed in this region, which indicates that there is dissolution of calcite and dolomite or cation exchange. Most groundwater samples were distributed above 4:1, indicating a lack of Ca^{2+} in this region, excessive HCO_3^- , and the possibility of desulfurization (Eq. 5) or cation exchange (Ren et al. 2021).



According to Eq. (6), if Ca^{2+} and SO_4^{2-} are purely derived from gypsum dissolution, then $\rho(\text{Ca}^{2+})/\rho(\text{SO}_4^{2-}) = 1$ (Wu et al. 2014). The groundwater samples of the three aquifers are mainly distributed in the upper part of the 1:1 line, where Ca^{2+} is insufficient relative to SO_4^{2-} , and pyrite oxidation (Eq. 7) and cation exchange may occur (Fig. 6c).



The values of $\rho(\text{Na}^+)/\rho(\text{Cl}^-)$ are usually used to reveal the source of Na^+ in groundwater. If $\rho(\text{Na}^+)/\rho(\text{Cl}^-) = 1$ (Eq. 8), the Na mainly comes from halite dissolution (Liu et al. 2019; Yuan et al. 2017). Only two groundwater samples from the Carboniferous aquifer lie in the upper part of the 1:1 line; the others are all below the 1:1 line, indicating that in addition to dissolution of rock salt, cation exchange is occurring in the three aquifers (Fig. 6d).



The values of $\rho(\text{Na}^+ - \text{Cl}^-)/\rho[(\text{Ca}^{2+} + \text{Mg}^{2+}) - (\text{HCO}_3^- + \text{SO}_4^{2-})]$ are used to judge cation exchange in groundwater (Chen et al. 2019). When groundwater containing Ca^{2+} and Mg^{2+} flows through the rock, the Na^+ on the rock surface is replaced by Ca^{2+} and Mg^{2+} , increasing the Na^+ concentration and decreasing the Ca^{2+} and Mg^{2+} concentrations in the water. As shown in Fig. 7e, all groundwater samples are close to the $\rho(\text{Na}^+ - \text{Cl}^-)/\rho[(\text{Ca}^{2+} + \text{Mg}^{2+}) - (\text{HCO}_3^- + \text{SO}_4^{2-})] = -1$ reference line; compared with SO_4^{2-} and HCO_3^- , Ca^{2+} and Mg^{2+} in the three aquifers are insufficient (Fig. 7a). Therefore, cation exchange is occurring.

The values of $\rho(\text{SO}_4^{2-})/\rho(\text{Cl}^-)$ usually reflect groundwater desulfurization (He et al. 2020). The less the value

of $\rho(\text{SO}_4^{2-})/\rho(\text{Cl}^-)$, the stronger the desulfurization. Meanwhile, the smaller the value of $\rho(\text{SO}_4^{2-})/\rho(\text{Cl}^-)$, the slower the groundwater flow. A value of $\rho(\text{SO}_4^{2-})/\rho(\text{Cl}^-) = 0$ means that the desulfurization is complete (Xu et al. 2020). Most groundwater samples fell below the 1:1 line (Fig. 6f). The $\rho(\text{SO}_4^{2-})/\rho(\text{Cl}^-)$ value order was the: Neogene aquifer > Carboniferous aquifer > Permian aquifer. Since there is no carbon source in the Neogene aquifer, there is almost no desulfurization. The sandstone groundwater in the roof of the coal measure strata is a reducing environment with slow flow, which provides appropriate conditions for desulfurization. Most of the Permian aquifer groundwater samples had $\rho(\text{SO}_4^{2-})/\rho(\text{Cl}^-)$ values less than 0.04, which indicates that the Permian aquifer is relatively closed, and there is a strong desulfurization in some parts of the study area. The $\rho(\text{SO}_4^{2-})/\rho(\text{Cl}^-)$ values of the groundwater samples from the Carboniferous aquifer is medium; the Carboniferous aquifer has a hydraulic connection with the Neogene aquifer in the shallow outcrop, and the carbon source is less, so the desulfurization is weak.

Discussion

Generalization of the Groundwater Flow Field

The flow direction of groundwater can be identified by assuming a sufficient water supply. A relatively short water–rock interaction is associated with small TDS values, and water–rock interactions and TDS values tend to increase along the flow direction of groundwater (Chen et al. 2014; Jiang 2020). The TDS contour maps of the three aquifers are drawn by SURFER 9.0 (Fig. 7a–c). The TDS values of the Neogene aquifer are relatively high and gradually increase from the northeast to the southwest of the study area, so the general flow direction of the Neogene aquifer is from the northeast of the study area to the southwest (Fig. 7a). The TDS values of the Permian and Carboniferous aquifers are relatively low and have not changed much, gradually increasing from the southwest to the northeast of the study area. Therefore, the general flow direction of the Permian and Carboniferous aquifers is from the southwest to the northeast (Fig. 7b, c).

The Main Controlling Factors of the Hydrochemical Field

Generally, one of two methods are used to extract the number of principal components: extracting those with eigenvalues greater than 1 or those with a cumulative contribution of 85% (Tai et al. 2005). We used the second method to select the first three principal components. As shown in Table 2 and Fig. 8, principal component 1 (F1) explains

Fig. 7 TDS contour map of three aquifers in the study area: **a** the Neogene aquifer; **b** the Permian aquifer; **c** the Carboniferous aquifer

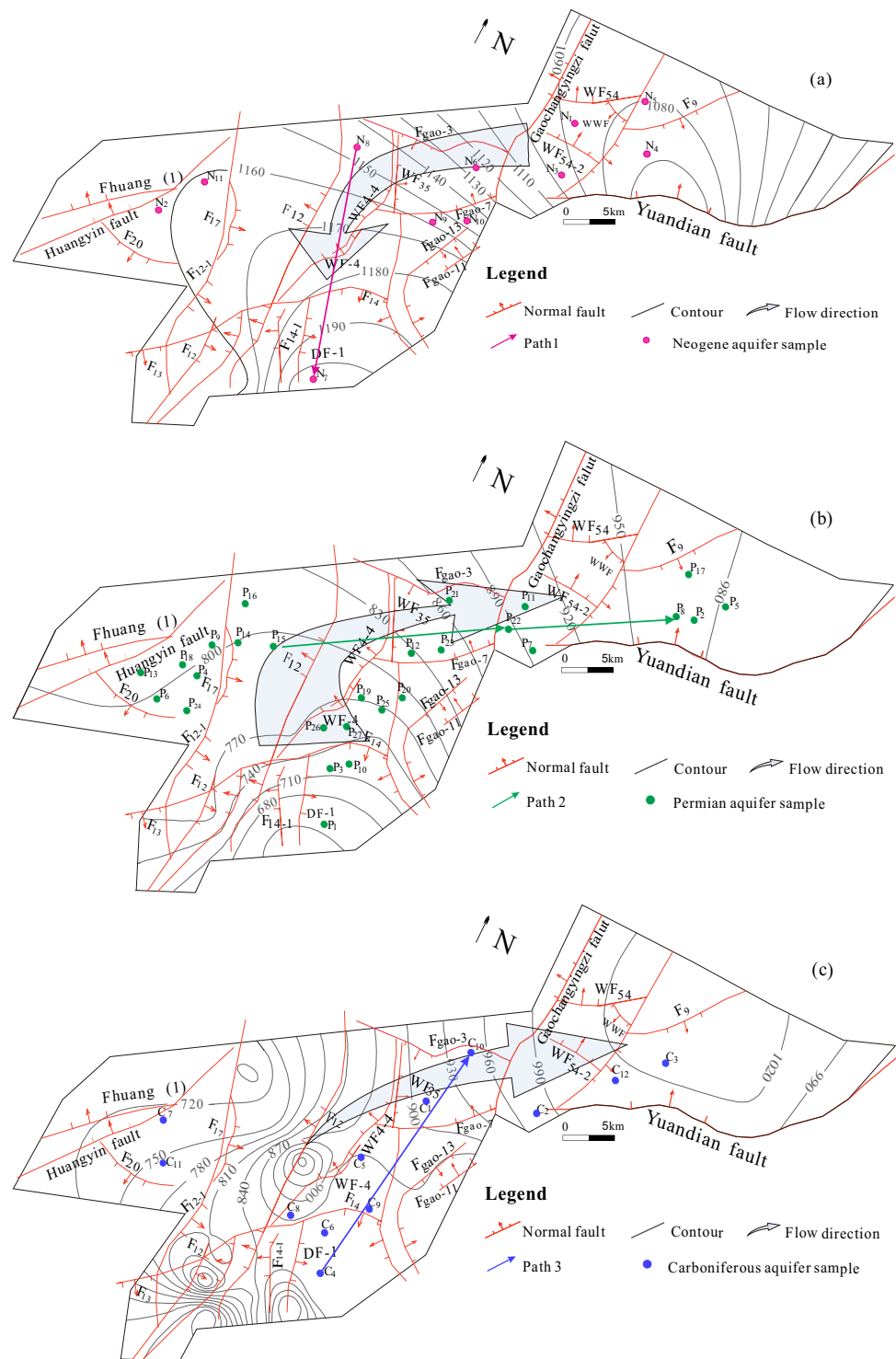


Table 2 Eigenvalues of the correlation matrix

Factor	Eigenvalue	Contribution rate%	Cumulative%
F1	2.77	46.15	46.151
F2	1.71	28.43	74.582
F3	0.84	13.95	88.530
F4	0.56	9.39	97.923
F5	0.11	1.75	99.675
F6	0.02	0.33	100.000

and SO_4^{2-} accounted for the negative load, which is due to desulfurization. Therefore, principal component 1 (F1) represents dissolution of carbonate minerals and gypsum and pyrite oxidation, principal component 2 (F2) represents dissolution of halite and cation exchange, and principal component 3 (F3) represents pyrite oxidation.

The principal component load scores of the groundwater samples are plotted as a scatter diagram (Fig. 9). The load scores of F1, F2, and F3 are expressed by SF1, SF2, and SF3, respectively. The groundwater samples from the Neogene aquifer all fall in the first quadrant of Fig. 9a–c, but the score on the F3 axis is low, which indicates that dissolution of carbonate minerals, gypsum, and halite, and

cation exchange greatly influence the Neogene aquifer. Most of the Permian aquifer samples fall in the second quadrant of Fig. 9a, b, and some fall in the third quadrant of Fig. 9a, b, which indicates that the hydrogeochemical processes in the Permian aquifer mainly include cation exchange, dissolution of halite, and desulfurization, while the hydrogeochemical processes in some of the Permian aquifer samples are more subtle. The Carboniferous aquifer samples are mainly distributed in the second quadrant of Fig. 9a, b, indicating that the main hydrogeochemical processes of the Carboniferous aquifer are dissolution of carbonate minerals, gypsum, and pyrite oxidation, though dissolution of halite and cation exchange also influences this aquifer.

Hydrochemical Field Evolution Analyses

Neogene Aquifer Evolution

The groundwater samples from the Neogene aquifer all have SF1, SF2, and SF3 scores greater than 0 (Fig. 10a). In and near the northeast of the study area, the SF1 is higher and the SF2 is lower. This is because groundwater flows rapidly near the eastern recharge area, so dissolution of carbonate minerals and gypsum is strong, while cation exchange is weak. Along the groundwater

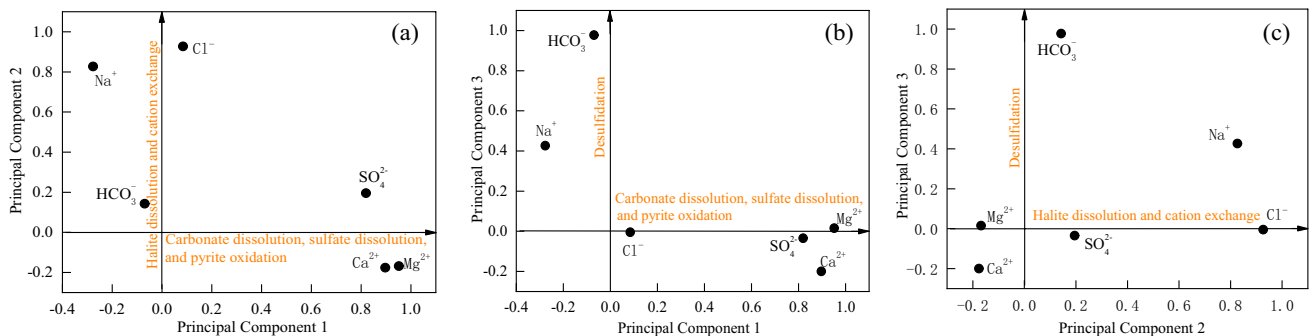
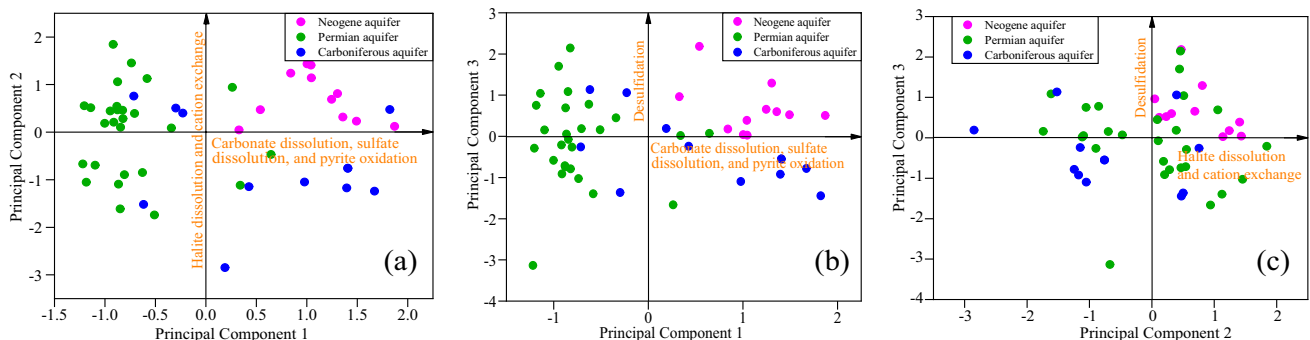
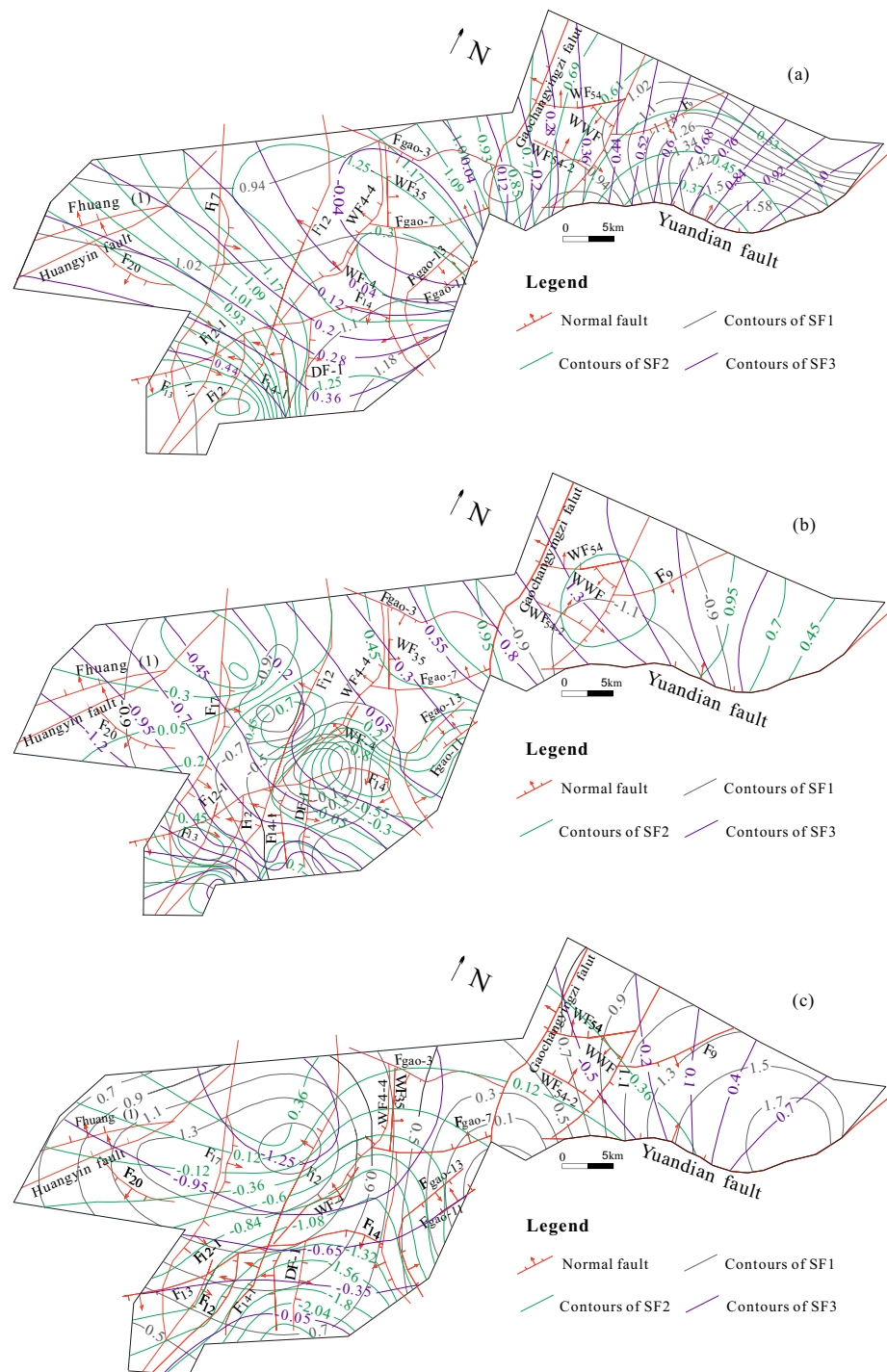
**Fig. 8** Principal components load: **a** F1 and F2, **b** F1 and F3, **c** F2 and F3**Fig. 9** Load scores of principal components of the groundwater samples: **a** SF1 and SF2, **b** SF1 and SF3, **c** SF2 and SF3

Fig. 10 Contour maps of principal component scores (SF1, SF2, SF3) in the three aquifers: **a** the Neogene aquifer, **b** the Permian aquifer, **c** the Carboniferous aquifer



flow path, SF1 decreases and SF2 increases due to the slow water flow in the southwest drainage area, which reduces dissolution and enhances cation exchange. The SF3 of the Neogene aquifer is low, because as previously mentioned, the lack of a carbon source makes desulfurization difficult.

Permian Aquifer Evolution

The main component load scores of the Permian aquifer have obvious spatial differences. SF1 of the Permian aquifer is negative, while SF2 and SF3 are mostly positive (Fig. 10b). Due to the Gaochangyingzi and Yuandian faults, the aquifer is relatively closed, and groundwater flow is slow, which

weakens dissolution. However, the closed environment provides favorable conditions for desulfurization and cation exchange. The faults and small structures are relatively well developed in the southwest. Affected by faults F12, F13, F14, F17, and WF-4, the aquifer is relatively open, dissolution of carbonate minerals and gypsum is enhanced, and desulfurization as well as dissolution of halite and cation exchange are all weak. Therefore, the regional geological structure controls the hydrogeochemical processes of this aquifer.

Carboniferous Aquifer Evolution

The SF1 of the Carboniferous aquifer exceeds 0, while SF2 and SF3 are less than 0 (Fig. 10c). Similar to the Permian aquifer, the SF1 of the Carboniferous aquifer is lower in the northeast than in the southwest, while SF2 and SF3 are higher in the northeast than in the southwest. In the northeast, due to the influence of the Gaochangyingzi and Yuan-dian faults, the groundwater flow is stagnant, which weakens dissolution of carbonate minerals and gypsum and pyrite oxidation. Meanwhile, the aquifer is closed, and water–rock interaction is prolonged, which enhances cation exchange and desulfurization. The aquifer in the southwest is relatively open. Dissolution of carbonate minerals and gypsum and pyrite oxidation are enhanced, while cation exchange and desulfurization are weakened.

Along the groundwater flow path, the hydrogeochemistry of the Carboniferous aquifer in the study area presents a certain regularity. SF1 in the southwest recharge area is higher than in the northeast discharge area, and SF2 and SF3 are lower than in the discharge area. Because the groundwater flow velocity in the recharge area is fast, dissolution is strong, the time of water–rock interaction is short, and the cation exchange and desulfurization are weak. Thus, the hydrogeochemical processes of the Carboniferous aquifer are controlled by both the groundwater flow conditions and regional geological structures.

Hydrogeochemical Inverse Modeling

Hydrogeochemical inverse modeling determines the amount of mineral dissolution or precipitation between two points on a groundwater flow line by identifying and quantifying

the hydrogeochemical reactions using the composition of groundwater and rock to explain the hydrogeochemical processes (Chen et al. 2020). Normally, PHREEQC 3.0 is used for hydrogeochemical inverse modeling; the selection of path and possible reaction phases is the key to modeling. Since the modeling path is determined by the flow direction, and water–rock interaction and TDS values increase along the groundwater flow direction, the modeling path is selected using the spatial distribution of the TDS. Each modeling path contains two sample points; finally, three simulation paths are determined (Fig. 7a–c).

According to the hydrogeological conditions, aquifer lithology, and water quality analysis results, calcite, dolomite, gypsum, and halite were selected as the main water–rock reaction phases. NaX and CaX₂ represent cation exchange. In addition, CO₂ is involved in the whole processes of carbonate mineral dissolution and is also used as the input phase of the model. H₂S represents desulfurization and O₂ represents pyrite oxidation.

- (1) Path 1: For the Neogene aquifer, the water chemistry of points Q7 and Q8 were used for the inverse modeling (Path 1, Fig. 7a, Table 3). It can be seen that only a small amount of gypsum dissolved. Cation exchange resulted in the release of Na⁺ and the absorption of Ca²⁺. The precipitation of calcite, dolomite, and halite reduced the concentrations of Ca²⁺, HCO₃[−], and Cl[−] in the groundwater. In the above analysis. The discussion results of ions ratios analysis and principal component analysis show that the hydrogeochemical process of Neogene aquifer includes carbonate minerals dissolution, gypsum dissolution and cation exchange, and the spatial interpolation analysis of principal component scores shows that dissolution is weakened and the cation exchange is enhanced along the flow direction of groundwater in the Neogene aquifer. These inverse modeling results are consistent with the qualitative analysis results reported earlier.
- (2) Path 2: For the Permian aquifer, the water chemistry of points P15, P22, and P8 were used for the inverse modeling (Path 2, Fig. 7b, Table 3). The modeling results of path 2 show that along both parts of the path, gypsum dissolves, halite and dolomite dissolves or precipitates,

Table 3 Calculated results of inverse modeling on path (units: mmol/L)

Aquifers	Path	Calcite	CaX ₂	Gypsum	NaX	CO ₂ (g)	Halite	Dolomite	H ₂ S(g)	O ₂ (g)
Neogene aquifer	Q7 → Q8	− 0.284	− 0.352	0.512	0.703	1.984	− 1.168	− 0.249	−	−
Permian aquifer	P15 → P22	−	− 0.628	0.410	1.256	3.028	− 2.049	0.298	− 0.154	− 0.308
	P22 → P8	−	− 0.416	0.754	0.832	2.335	2.969	− 0.454	− 1.537	− 3.075
Carboniferous aquifer	C4 → C10	− 1.592	− 0.465	1.527	0.931	−	− 3.144	1.011	0.420	0.841

Positive value indicates mineral dissolution, negative value indicates mineral precipitation

and dissolution is weak. Both results confirmed cation exchange. The escape of H_2S gas explained the occurrence of desulfurization in the Permian aquifer. In the above analysis. The discussion results of ions ratios analysis and principal component analysis show that the hydrogeochemical process of the Permian aquifer mainly includes cation exchange, pyrite oxidation, desulfurization and dissolution, and the spatial interpolation analysis of principal component scores shows that the cation exchange and desulfurization are enhanced, and pyrite oxidation and dissolution are weakened along the flow direction of groundwater in the Permian aquifer. The modeling results are consistent with the above qualitative analysis results.

- (3) Path 3: For the Carboniferous aquifer, the water chemistry of the two points C14 and C10 are selected in the inverse modeling (Path 3, Fig. 7c, Table 3). The modeling results of path 3 show that along the flow path, gypsum and dolomite dissolves and calcite and halite are precipitates, and dissolution is weak. The results confirmed the occurrence of cation exchange and the weak pyrite oxidation. In the above analysis. The results of ion ratio analysis and principal component analysis show that the hydrogeochemical process of the Carboniferous aquifer mainly includes pyrite oxidation, cation exchange, and dissolution. The spatial interpolation analysis of principal component scores shows that the dissolution and pyrite oxidation are weakened along the groundwater flow, and the cation exchange and desulfurization are enhanced along the flow direction of groundwater in the Carboniferous aquifer. The quantitative analysis results of the modeling support the above qualitative analysis.

Conclusion

In this study, the hydrogeochemical processes and its controlling factors of the main water-inrush aquifers in the Yuaner coal mine were studied by conventional hydrochemistry methods, principal component analysis, and hydrogeochemical inverse modeling. The following conclusions were gained.

- (1) The hydrochemical types of the Neogene aquifer are mainly HCO_3-Na , $HCO_3-Cl-Na$, $Cl-HCO_3-Na$, and $Cl-Na$. The hydrochemical types of the Permian aquifer are mainly HCO_3-Na , $HCO_3-Cl-Na$, and $Cl-HCO_3-Na$. The hydrochemical types of the Carboniferous aquifer are mainly $Cl-HCO_3-Na$, HCO_3-Na , $Cl-Na$, $HCO_3-Na-Ca$, and $HCO_3-Cl-Na$. Gibbs plot analysis

shows that the hydrochemical composition in the study area is mainly controlled by water–rock interaction.

- (2) According to ion ratio analysis, principal component analysis, and the spatial interpolation analysis, the hydrogeochemical processes and the factors controlling the aquifers differ. In the Neogene aquifer, the main hydrogeochemical processes are cation exchange, dissolution of calcite, dolomite, and gypsum. The Neogene aquifer is affected by the mineral compositions of the aquifer and the flow condition of groundwater. Along the flow path of groundwater, dissolution of calcite, dolomite and gypsum changes from strong to weak; in contrast, the cation exchange changes from weak to strong. In the Permian aquifer, the main hydrogeochemical processes are desulfurization and cation exchange. The Permian aquifer is influenced by regional geological structures; dissolution and pyrite oxidation are strong, and desulfurization and cation exchange are weak due to small geologic structures developed in the southwest, while the dissolution is weak, and desulfurization and cation exchange are strong in the northeast. In the Carboniferous aquifer, the main hydrogeochemical processes are dissolution of calcite, dolomite, and gypsum, and pyrite oxidation; cation exchange is a secondary hydrogeochemical process. The Carboniferous aquifer is influenced by groundwater flow conditions and regional geological structures; mineral dissolution and pyrite oxidation are stronger, while cation exchange and desulfurization are weaker in the southwest. Along the groundwater flow direction, mineral dissolution is weakened, and cation exchange is enhanced in the northeast.
- (3) The main water–rock interactions along the groundwater flow path were quantitatively analyzed using hydrogeochemical inverse modeling. According to the inverse modeling results, cation exchange and weak dissolution occur along the flow path in the Neogene aquifers. The modeling results of the Permian aquifer confirm the occurrence of cation exchange and desulfurization in this aquifer, and mineral dissolution is weak. In addition, cation exchange, weak mineral dissolution, and pyrite oxidation were confirmed to be occurring in the Carboniferous aquifer. The inverse modeling results were consistent with the qualitative analysis results of conventional hydrochemistry methods and principal component analysis.

Supplementary Information The online version contains supplementary material available at <https://doi.org/10.1007/s10230-022-00851-0>.

Acknowledgements This paper was supported by the National Natural Science Foundation of China (grant 41972256). The authors thank

the anonymous reviewers for their careful comments and useful suggestions.

Funding This article was funded by National Natural Science Foundation of China (Grant no. 41972256).

References

- Banning A, Demmel T, Rude TR, Wrobel M (2013) Groundwater uranium origin and fate control in a river valley aquifer. *Environ Sci Technol* 47(24):13941–13948. <https://doi.org/10.1021/es304609e>
- Belkhir L, Mouni L, Tiri A (2013) Water-rock interaction and geochemistry of groundwater from the Ain Azel. *Environ Geochem Health* 34(1):1–13. <https://doi.org/10.1007/s10653-011-9376-4>
- Bridge G (2004) Contested terrain: mining and the environment. *Ann Rev Environ Res* 29:205–259. <https://doi.org/10.1146/annurev.energy.28.011503.163434>
- Chen LW, Xu DQ, Yin XX, Xie WP, Zeng W (2017) Analysis on hydrochemistry and its controlling factors in the concealed coal mining area in north China: a case study of dominant inrush aquifers in Suxian mining area. *J China Coal Soc* 42(4):996–1004. <https://doi.org/10.13225/j.cnki.jccs.2016.0685> (in Chinese)
- Chen LW, Yin XX, Xie WP, Feng XQ (2014) Calculating groundwater mixing ratios in groundwater-inrushing aquifers based on environmental stable isotopes (D, ^{18}O) and hydrogeochemistry. *Nat Hazards* 71(1):937–953. <https://doi.org/10.1007/s11069-013-0941-2>
- Chen JP, Zhu JC, Yin XC, Lv XM, Sun HF (2020) Discrimination of mine water-inrush source based on PHREEQC inverse analysis-cluster analysis method. *Coal Technol* 39(11):75–78. <https://doi.org/10.13301/j.cnki.ct.2020.11.021>
- Chen Y, Zhu SY, Xiao SJ (2019) Discussion on controlling factors of hydrogeochemistry and hydraulic connections of groundwater in different mining districts. *Nat Hazards* 99(2):689–704. <https://doi.org/10.1007/s11069-019-03767-1>
- Chotpanarat S, Thamrongsrisakul J (2021) Natural and anthropogenic factors influencing hydrochemical characteristics and heavy metals in groundwater surrounding a gold mine. *Thailand J Asian Earth Sci* 211:104692. <https://doi.org/10.1016/j.jseaes.2021.104692>
- Fijani E, Moghaddam AA, Tsai FTC, Tayfur G (2017) Analysis and assessment of hydrochemical characteristics of Maragheh-Bonab plain aquifer, northwest of Iran. *Water Resour Manag* 31(3):765–780. <https://doi.org/10.1007/s11269-016-1390-y>
- Gastmans D, Chang HK, Hutcheon I (2010) Groundwater geochemical evolution in the northern portion of the Guarani aquifer system (Brazil) and its relationship to diagenetic features. *Appl Geochem* 25(1):16–33. <https://doi.org/10.1016/j.apgeochem.2009.09.024>
- Guo Y, Gui HR, Wei JC, Zhang Z, Hu MC, Fang P, Li GP, Gao C, Wang X (2020) Hydrogeochemistry of water in coal measures during grouting treatment of Taoyuan Mine. *China Groundwater* 56(2):256–269. <https://doi.org/10.1111/gwat.13038>
- Han Y, Wang G, Cravotta CA, Hu WY, Bian YY, Zhang ZW, Liu YY (2013) Hydro-geochemical evolution of Ordovician limestone groundwater in Yanzhou, north China. *Hydrol Process* 27(16):2247–2257. <https://doi.org/10.1002/hyp.9297>
- He S, Li P (2020) A MATLAB based graphical user interface (GUI) for quickly producing widely used hydrogeochemical diagrams. *Geochemistry* 80(4):125550. <https://doi.org/10.1016/j.chemer.2019.125550>
- He SF, Cheng YC, Xie H, An YQ, Jiang CL, Zheng L (2020) Water chemistry characteristics and their causes of limestone groundwater in Panxie Mining Area. *Energy Environ Protection* 34(01):37–43 (in Chinese)
- Huang PH, Han SM (2017) Study of multi-aquifer groundwater interaction in a coal mining area in China using stable isotopes and major-ion chemical data. *Environ Earth Sci* 76(1):17. <https://doi.org/10.1007/s12665-016-6310-1>
- Huang XJ, Wang GC, Liang XY, Gui LF, Ma L, Xu QY (2017) Hydrochemical and stable isotope (δD and $\delta^{18}\text{O}$) characteristics of groundwater and hydrogeochemical processes in the Ningxiaota coalfield northwest China. *Mine Water Environ* 37(1):119–136. <https://doi.org/10.1007/s10230-017-0477-x>
- Hu SY, Zhao QS, Wang GC, Zhang JW, Feng J (2018) Hydrochemical dynamic characteristics and evolution of underground brine in the Mahai Salt Lake of the Qaidam Basin Qinghai-Tibet Plateau. *Acta Geol Sin* 92(5):1981–1990. <https://doi.org/10.1111/1755-6724.13690>
- Ibrahim RGM (2020) Geochemical simulation of the hydrogeochemical processes affecting groundwater quality of the Eocene aquifer east of El Minia Governorate-Eastern desert-Egypt. *J Afr Earth Sci* 174:104097. <https://doi.org/10.1016/j.jafrearsci.2020.104097>
- Ismail E, Abou Heleika M (2021) Hydrochemical characteristics and quality assessment of groundwater aquifers northwest of Assiut district. *Egypt J African Earth Sci* 181:104260. <https://doi.org/10.1016/j.jafrearsci.2021.104260>
- Jiang XF (2020) Reverse hydrogeochemical simulation of Cambrian limestone aquifer in Ping Dingshan mining area. *Groundwater* 42(06):1–4. <https://doi.org/10.19807/j.cnki.DXS.2020-06-001> (in Chinese)
- Kaown D, Koh EH, Mayer B, Ju Y, Kim J, Lee HL, Lee SS, Park DK, Lee KK (2021) Differentiation of natural and anthropogenic contaminant sources using isotopic and microbial signatures in a heavily cultivated coastal area. *Environ Pollut* 273:116493. <https://doi.org/10.1016/j.envpol.2021.116493>
- Kumar P, Singh AK (2020) Hydrogeochemistry and quality assessment of surface and sub-surface water resources in Raniganj coalfield area, Damodar Valley, India. *Int J Environ Anal Chem* 2020:1–24. <https://doi.org/10.1080/03067319.2020.1849653>
- Li P, Qian H, Wu J, Zhang Y, Zhang H (2013) Major ion chemistry of shallow groundwater in the Dongsheng Coalfield, Ordos Basin. *China Mine Water Environ* 32(3):195–206. <https://doi.org/10.1007/s10230-013-0234-8>
- Li PY, Wu J, Tian R, He S, He X, Xue C, Zhang K (2018) Geochemistry, hydraulic connectivity and quality appraisal of multilayered groundwater in the Hongdunzi coal mine, northwest China. *Mine Water Environ* 37(2):222–237. <https://doi.org/10.1007/s10230-017-0507-8>
- Li W, Wu J, Zhou C, Nsabimana A (2021) Groundwater pollution source identification and apportionment using PMF and PCA-APCS-MLR receptor models in Tongchuan City. *China Arch Environ Contam Toxicol* 81(3):397–413. <https://doi.org/10.1007/s00244-021-00877-5>
- Liu P, Yang M, Sun YJ (2019) Hydrogeochemical processes of the deep Ordovician groundwater in a coal mining area. *Xuzhou China Hydrogeol J* 27(6):2231–2244. <https://doi.org/10.1007/s10040-019-01991-4>
- Luan FJ, Zhou JL, Jia RL, Lu CX, Bai M, Liang HT (2019) Hydrochemical characteristics and formation mechanism of groundwater in plain areas of Barkol-Yiwu Basin, Xinjiang. *Environ Chem* 36(02):380–389. <https://doi.org/10.7524/j.issn.0254-6108.2017.02.2016062001> (in Chinese)
- Malov AI, Tokarev IV (2019) Using stable isotopes to characterize the conditions of groundwater formation on the eastern slope of the Baltic Shield (NW Russia). *J Hydrol* 578:124130. <https://doi.org/10.1016/j.jhydrol.2019.124130>
- Marandi A, Shand P (2018) Groundwater chemistry and the Gibbs diagram. *Appl Geochem* 97:209–212
- Paternoster M, Buccione R, Canora F, Buttitta D, Panebianco S, Rizzo G, Sinisi R, Summa V, Mongelli G (2021) Hydrogeochemistry

- and groundwater quality assessment in the high Agri valley (southern Italy). *Geofluids* 2021:6664164. <https://doi.org/10.1155/2021/6664164>
- Qian H, Li P, Wu J, Zhou Y (2013) Isotopic characteristics of precipitation, surface and ground waters in the Yinchuan Plain, northwest China. *Environ Earth Sci* 70(1):57–70. <https://doi.org/10.1007/s12665-012-2103-3>
- Qiao W, Li WP, Zhang SC (2019) Effects of coal mining on the evolution of groundwater hydrogeochemistry. *Hydrogeol J* 27(6):2245–2262. <https://doi.org/10.1007/s10040-019-01969-2>
- Ren X, Li P, He X, Su F, Elumalai V (2021) Hydrogeochemical processes affecting groundwater chemistry in the central part of the Guanzhong Basin. *China Arch Environ Contam Toxicol* 80(1):74–91. <https://doi.org/10.1007/s00244-020-00772-5>
- Sako A, Bamba O, Gordio A (2016) Hydrogeochemical processes controlling groundwater quality around Bomboré gold mineralized zone, central Burkina Faso. *J Geochem Explor* 170:58–71. <https://doi.org/10.1016/j.gexplo.2016.08.009>
- Shen ZL, Zhu WH, Zuo SZ (1999) Hydrogeochemistry basics. Geology Press, Beijing, pp 101–110 (in Chinese)
- Tai SC, Sun WY, He JJ (2005) Applied Mathematical Statistics. Wuhan University Press, Wuhan, pp 248–256 (in Chinese)
- Taufiq A, Hosono T, Ide K, Kagabu M, Iskandar I, Efendi AJ, Hutasoit L, Shimada J (2018) Impact of excessive groundwater pumping on rejuvenation processes in the Bandung basin (Indonesia) as determined by hydrogeochemistry and modeling. *Hydrogeol J* 26(4):1263–1279. <https://doi.org/10.1007/s10040-017-1696-8>
- Tian H, Du JZ, Ma SM, Kang Z, Gong Y (2020) Application of water quality index and multivariate statistical analysis in the hydrogeochemical assessment of shallow groundwater in Hailun, northeast China. *Hum Ecol Risk Assess* 27(3):651–667. <https://doi.org/10.1080/10807039.2020.1749827>
- Vaiphei SP, Kurakalva RM (2021) Hydrochemical characteristics and nitrate health risk assessment of groundwater through seasonal variations from an intensive agricultural region of upper Krishna River basin, Telangana. *India Ecotoxicol Environ Saf* 213:112073. <https://doi.org/10.1016/j.ecoenv.2021.112073>
- Wang D, Wu J, Wang Y, Ji Y (2020) Finding high-quality groundwater resources to reduce the hydatidosis incidence in the Shiqu County of Sichuan Province, China: analysis, assessment, and management. *Expo Health* 12(2):307–322. <https://doi.org/10.1007/s12403-019-00314-y>
- Wu JH, Li PY, Qian H, Duan Z, Zhang XD (2014) Using correlation and multivariate statistical analysis to identify hydrogeochemical processes affecting the major ion chemistry of waters: a case study in Laoheba phosphorite mine in Sichuan. *China Arab J Geosci* 7(10):3973–3982. <https://doi.org/10.1007/s12517-013-1057-4>
- Wu J, Li P, Qian H (2015) Hydrochemical characterization of drinking groundwater with special reference to fluoride in an arid area of China and the control of aquifer leakage on its concentrations. *Environ Earth Sci* 73(12):8575–8588. <https://doi.org/10.1007/s12665-015-4018-2>
- Wu J, Li P, Wang D, Ren X, Wei M (2020) Statistical and multivariate statistical techniques to trace the sources and affecting factors of groundwater pollution in a rapidly growing city on the Chinese Loess Plateau. *Hum Ecol Risk Assess* 26(6):1603–1621. <https://doi.org/10.1080/10807039.2019.1594156>
- Xu GQ, Wang L, Gao YH, Su Y, Li YH (2020) Analysis on the hydrogeochemical characteristics and formation mechanism of 13–1 coal seam sandstone aquifer in the central part of Huainan mining area. *J Anhui Univ Sci Tech (nat Sci)* 40(06):27–34 (in Chinese)
- Yang F, Liu S, Jia C, Gao MS, Chang WB, Wang YJ (2021) Hydrochemical characteristics and functions of groundwater in southern Laizhou Bay based on the multivariate statistical analysis approach. *Estuar Coast Shelf Sci* 250:107153. <https://doi.org/10.1016/j.ecss.2020.107153>
- Yuan JF, Xu F, Deng GS, Tang YQ, Li PY (2017) Hydrogeochemistry of shallow groundwater in a karst aquifer system of Bijie City. *Guizhou Province Water* 9(8):625. <https://doi.org/10.3390/w9080625>
- Zhai JT, Li L, Wang J L (2013) Research on tectonic control of gas occurrence in Yuandian no. 2 Mine. *Min Saf Env Protect* 40(03):96–99 (in Chinese)
- Zhang HT, Xu GQ, Chen XQ, Mabaire A, Zhou JS, Zhang YX (2019a) Groundwater hydrogeochemical processes and the connectivity of multilayer aquifers in a coal mine with karst collapse columns. *Mine Water Environ* 39(2):356–368. <https://doi.org/10.1007/s10230-020-00667-w>
- Zhang HT, Xu GQ, Chen XQ, Mabaire A (2019b) Hydrogeochemical evolution of multilayer aquifers in a massive coalfield. *Environ Earth Sci* 78(24):675. <https://doi.org/10.1007/s12665-019-8694-1>
- Zhang HT, Xu GQ, Chen XQ, Wei J, Yu ST, Yang TT (2019c) Hydrogeochemical characteristics and groundwater-inrush source identification for a multi-aquifer system in a coal mine. *Acta Geol Sin* 93(6):1922–1932. <https://doi.org/10.1111/1755-6724.14299>
- Zhang HT, Xu GQ, Zhan HB, Chen XQ, Liu MC, Wang MH (2020) Identification of hydrogeochemical processes and transport paths of a multi-aquifer system in closed mining regions. *J Hydrol* 589:125344. <https://doi.org/10.1016/j.jhydrol.2020.125344>
- Zhang J, Chen LW, Li J, Chen YF, Ren XX, Shi XP (2021) Analysis of mining effects on the geochemical evolution of groundwater, Huaibei coalfield. *China Environ Earth Sci* 80(3):98. <https://doi.org/10.1007/s12665-021-09399-8>
- Zhu NN (2018) Safety pillar design for coal-caving under aquifer of 83 mining area, Yuandian no. 2 coalmine. MA Eng Diss, Anhui Univ of Science and Technology (in Chinese)